Fragility of Bridge Decks exposed to Hydraulic and Driftwood Actions

Alessandro Pucci[a]*, Hélder S. Sousa[a], Linda Giresini[b], José C. Matos[a] and Fabio Castelli[c]

[a] *University of Minho, ISISE, ARISE, Department of Civil Engineering, Guimarães, Portugal;*

[b]*Department of Structural and Geotechnical Engineering, Sapienza University of Rome, Italy;*

[c]*Department of Civil and Environmental Engineering, University of Florence, Florence, Italy;*

*Corresponding Author; email: ale@civil.uminho.pt

A resilient bridge network is vital to a community recovery after natural disasters. Floods are the main cause of bridge collapses, but there is little research on the combined fragility of single-span bridge decks to hydrodynamic forces and driftwood clogging. Moreover, most studies concentrate on multi-span bridges and piers. By using HEC-RAS software and in-house developed Python scripts, this work proposes a method to obtain fragility curves for single-span bridges accounting for hydrodynamic actions and driftwoods. Due to the lack of indications from standards concerning uplift and overturning of bridge decks, these limit states are included in the formulation together with slippage. Results revealed that all three limit states must be taken into account and showed that driftwood clogging can have a severe impact on the failure probability of the bridge, with even a minor decrease in clearance causing a significant safety reduction. Additionally, this work discusses the influence of hydrologic model recalibration on the failure probability of a structure.

Keywords: fragility Curves; Driftwood clogging; Floods; hydrodynamic Actions; single-span Bridges; HEC-RAS.

1. Introduction

Bridges are gateways for people and goods even during and after natural hazard events, such as floods, earthquakes, and wildfires. At infrastructural level, it is desirable to have a resilient and robust bridge network to avoid isolation of communities in case of disruptions (Han & Frangopol, 2022). Therefore, bridge collapses are widely studied, forasmuch as flood-related ones constitute the majority of such occurrences (Proske, 2018). This paper sheds light on the effects of hydraulic actions on bridge decks, including driftwoods clogging, using a probabilistic approach.

The analysis of hydrodynamic actions on bridge design underlines the possibility that the deck freeboard might be closed up by a range of discharges. This event can be amplified by driftwoods clogging. Examples of designs accounting for overtopping events can be found in Australia, where the Australian Standards 5100 prescribes checks against such occurrences (Committee BD-090, 2017). More often, especially in Europe, bridges are not designed to sustain water thrust against decks, while it is only advised the designer to provide an adequate freeboard as for the design peak discharge (CEN, 2005). This gap between the water surface and the girder soffit acts as a safety factor relatively to the uncertainty affecting the discharge. In the last decades, due to a combination of climatic changes and lack of maintenance, failures due to overtopping/dragging are increasingly reported (Oudenbroek et al., 2018). This highlighted the need for further investigations to assess and prevent these failure mechanisms. Up to date, only the Australian Bridge Design Code AS5100 considers variable hydrodynamic coefficients, while Eurocode 1 and AASHTO use a constant value and only for drag, neglecting both uplift and overturning limit states (CEN, 2005; AASTHO, 2012). In the case of Eurocode 1, such limit state is to be considered only during the construction phase. Despite such differences, all the mentioned standards define the action in a similar way, i.e. using coefficients to reproduce the effect of a dynamic action within a static framework. This

is mainly due to the complexity behind hydrodynamic coefficients. Indeed, despite a clear theoretical background, hydrodynamic coefficients are not easy to determine, even with numerical simulations, due to the deck-flow interaction. Conversely, flume experiments allow to segregate variables and identify the influence of each parameter on pressure coefficients (Kerenyi et al., 2009). Therefore, in this work results of experimental campaigns are employed to determine hydrodynamic coefficients at each water stage.

The other aspect to consider is the driftwood clogging. The term Large Wood (LW) is commonly referred to wood logs having length ≥ 1m and diameter ≥ 10cm (Schalko & Weitbrecht, 2022). Floating LW, known as driftwood is a key element to preserve the river ecosystem. On the other side, LW can pose serious threats to inline structures such as dams, weirs and bridges. It is therefore of paramount importance to implement administrative and engineering measures to reduce the risk at structures, while maintaining a sustainable river ecosystem. Among administrative measures, the subdivision of river's catchments into several hazard levels can be a cost-effective solution to implement early-warning systems (Schmocker & Weitbrecht, 2013). Recent approaches combine satellite imagery to quantify the clogging risk due to LW at bridges, including mitigation strategies (Panici & Kripakaran, 2023). Traditional engineering-based solutions involve the use of nets and racks to retain LW. But, also movable bridges and casings represent effective solutions (Schalko et al., 2020). A thoughtful discussion on impacts and mitigation measures of LW on river ecosystem can be found at relevant publication (Schalko & Weitbrecht, 2022). On the structural side, accumulation of LW at piers is particularly relevant for scour and backwater rise (Schalko et al., 2019). At single span bridges, the accumulation occurs against decks and flume setups involved both attaching a spanwise log mat to the deck as well as random clogging (Gschnitzer et al., 2017; Oudenbroek et al., 2018). The first strategy is focused on determining the increased

hydraulic forcing on the bridge deck, while the second is employed to determine the driftwood blocking probability. In this study, both strategies are used ~~, also~~ accounting ~~ed~~ ~~using~~ results of experimental campaigns for the blocking probability (Schmocker & Hager, 2011; Gschnitzer et al., 2017). Instead, the increased hydraulic thrust against the deck is analytically modelled as a worst-case scenario by using log mats, neglecting porosity due to limitations in the used software. In this perspective, ~~Hence,~~ the present work discusses actions not fully accounted in bridge design standards and shows how such unforeseen limit states can impact the safety of single-span bridges. To assess the safety level of the structure, fragility curves are derived. At the asset level, fragility functions represent failure probabilities of exceeding a certain structural threshold when subject to a given hazard magnitude (Porter et al., 2007). The methodologies to derive fragility curves can be subdivided in four groups: (i) analytical approaches; (ii) empirical methods; (iii) expert's judgement methods; (iv) hybrid approaches. Analytical approaches use numerical models to simulate the structural behaviour and hydraulic forcing, while empirical methods avail data from hazardous events, such as floods. Then, an analyst assesses the statistical significance of such information. Practitioners may also develop fragility functions based on available data and refine it by their judgement. As an example, weighted surveyed opinions may be used to influence the conditional damage probability based on a set of predefined questions designed to ensure consistency (Eidsvig et al., 2021). Combination of previous methods, called hybrid approaches, compensate for the lack of data (Allen et al., 2021), i.e. one can use an analytical method whose output can be refined by expert judgement. Traditionally, flood fragility analysis adopts an analytical approach, because data reliability and number of survey respondents hampers other methods. Present challenges of modelling flood fragility curves, emphasizing differences in flood treatment in a single or multi-hazard framework are described in

Section 2. Section 3 clarifies the assumptions and reviews concepts as hydrodynamic coefficients and driftwood ~~large wood~~ blocking probabilities. Section 4 introduces the stochastic vulnerability analysis by defining the limit states and consequently the bridge's conditional probability of failure. Section 5 applies the methodology to a case-study bridge located in Carrara, Italy. Section 6 presents the discussion of results, limitations of the present method as well as its future developments.

2. Literature Background

Many existing studies coupled floods with other hazards such as earthquakes, tsunamis, and long-term effects, i.e. corrosion (Li et al., 2020). Although floods impair - for example - the bridge seismic performance, recent studies revealed the importance of a dedicated hydraulic model (Argyroudis et al., 2019). Indeed, despite the consideration of hydrodynamic forces within the flood hazard, a river model in a multi-hazard fragility analysis it is still missing (Argyroudis & Mitoulis, 2021). The magnitude of hydraulic forces can impact bridges with effects similar to those generated by mild earthquakes (Li et al., 2020), but such actions are caused by the interaction between the river's conditions and the bridge (Dong & Frangopol, 2016). While simplified flood-bridge models reduce the computational cost, they cannot model the site-specific river behaviour (Khandel & Soliman, 2021). It is consequently necessary to develop flood-bridge impact models capable of analysing a problem at a desired level of detail with an affordable computational cost (D'Angelo et al., 2022).

2.1 River flow computation

A first issue concerns the estimation of the flow discharge magnitude. Rainfall-based approaches are commonly used to estimate discharges in the very frequent case of ungauged rivers. Among these, regional approaches offer a straightforward method to

compute river flow (Van Campenhout et al., 2020). Limitations consist mainly of their availability outside specific areas, e.g., the US (Yilmaz et al., 2016). Oversimplification and larger uncertainties on expected discharges occurs when the discharge return period is assumed equal to the rainfall's one (Gehl & D'Ayala, 2018), mainly because of the neglection of antecedent soil moisture conditions. On gauged rivers, issues arise from the length of hydrometric time series and possible upper boundary flow value due to a dam or weir in the bridge's proximity (Yilmaz et al., 2018). Another source of error is due to the possibility of water overtopping embankments, reducing the measured peak discharge. Newer methodologies try to link precipitation and temperature data with few measured discharges using Artificial Neural Networks or downscaling General Circulation Models (GCMs) (Khandel & Soliman, 2021). Distributed hydrological models stand out as being more efficient and of practical utility, as many local authorities adopted them for discharge calculation (Spyrou et al., 2020). Indeed, distributed Hydrological Models provide flood hazard characterization with several advantages that may reduce computational costs relative to downscaling GCMs or train an Artificial Neural Network, including higher spatial resolution in geodata, fewer analysis to parameters' variability, and promptness of outputs in readable GIS maps (Bizhanimanzar et al., 2020).

2.2 Hydrodynamic forces determination

When considering the structural analysis of a bridge, flood action can be split in static and dynamic components (Hamill, 1998). Flume experiments are often employed to determine the magnitude of dynamic thrusts on bridge decks by averaging the results of sensor readings on a predefined timeframe (e.g., 50s) (Dráb et al., 2019). Interestingly, lower discharges can lead to higher forces on structural components in specific cases, where dynamic components such as drag do not increase monotonically together with the

water height (Oudenbroek et al., 2018). Therefore, incremental water elevation simulations are preferable for a probabilistic analysis. This allows assessing structural safety at each step and not only at the highest water level. The incremental method has not applied to bridge decks yet, as in previous studies with such an approach the maximum water stage is kept below the deck level (Argyroudis et al., 2020). A selection of studies on flood fragility curves is presented in Table 1. It should be noted that driftwood blocking probability is not present in any of the referenced studies.

Table 1. Studies on flood fragility curves.

Intensity Measure	**N° Discharges**	**Hydrodynamic**	**Hydraulic model**
Velocity	1	AASHTO	No
Scour depth	6	No	No
Velocity	100 from Weibull distribution	AS 5100	No
Discharge	100 from 500 year rainfall	No	No
–	3 normal distributions	FHWA	No
Soil cover height	200 year return period	No	No
Discharge	100 from Weibull distribution	No	No
Discharge	ANN fitted on historical data	FEMA	No
Discharge and scour depth	7	AASHTO	HEC-RAS

Authors	(Kim et al., 2017)	(Tubaldi, Macorini, Izzuddin, et al., 2017)	(Kalendher et al., 2018)	(Lam et al., 2018)	(Mondoro & Frangopol, 2018)	(Tanasić & Hajdin, 2018)	(Lamb et al., 2019)	(Khandel & Soliman, 2021)	(Ahamed et al., 2021)

Not to be neglected, floods usually carry floating material and debris. When impacting bridges, drifting wood logs can pile at piers or at the deck, and they can be entrapped causing a backwater rise and a greater blockage area normal to the flow direction (Ruiz-Villanueva et al., 2017). The combination of these effects generates complex hydraulic forces that should be properly addressed in a vulnerability analysis.

2.3 Challenges in the modelling of wood logs occurrence

In this work, ~~large woods (~~LW~~)~~ are considered due to the damming effects that might lead the bridge to collapse. The log accumulation problem originates from catchments. LW budgeting and transport diagrams are available in related literature (Steeb et al., 2017). However, even without ~~budgeting~~ accounting LW ~~wood~~ recruitment, the most cost-effective strategy to minimize flood-related consequences is to reduce log jams at bridges (De Cicco et al., 2020). Study of past floods may provide hints about the expected amount of driftwood volume (De Cicco et al., 2018). Nevertheless, data collected during clogging processes typically concerns only accumulation at piers (Mazzorana et al., 2018). However, evidences show that log accumulation is possible also at bridges without piers (Schalko et al., 2017). Also in these scenarios, flume experiments play a key-role to understand the clogging mechanism. Limitations concern scale issues

on log samples' stiffness and their moisture content and, as pointed out by (De Cicco et al., 2018), this can overestimate the blocking probability. On the other hand, increasing the log sample smoothness underestimates the likelihood occurrence, balancing the two opposite effects. Indeed, field study on LW clogging showed that blocking probability as well as backwater rise are well modelled in flumes (Wyss et al., 2021). Conversely, log moisture content is still of major concern when retaining LW using for example a skimmer wall (Schalko, 2018). Other factors affecting the clogging process are: (i) water elevation (i.e. low freeboard), (ii) congested or uncongested transport of LW ~~woods~~ and (iii) existence of bridge elements with sharp edges, which can facilitate the entrapment (Gschnitzer et al., 2017). Gschnitzer et al. (2017), performed a logistic regression out of 5760 flume tests to compute the blocking probability of logs against bridge decks. Some tests included countermeasures such as a baffle installed on the upstream side of the deck and different shapes of logs (i.e. with and without branches). Another experimental study, performed by Schmocker & Hager, (2011), accounts for single log blocking probability, as tests demonstrated the significance of the first log entrapment on the jam formation. This process, unlike the one on piers, does not depend on the log orientation and once a single log gets trapped, the clogging process is not likely to revert (Panici & de Almeida, 2018). The blocking probability is furnished based on bridge features, log geometry and flow Froude number.

2.4 The role of software-based simulations

Alongside with flume experiments, software-based simulations are useful to assess the transport and deposition of drifting wood logs at catchment's scale (De Cicco et al., 2020). But further developments are needed concerning impacts on bridges. Given the scope and aims of this study, HEC-RAS was chosen as likely the most widely known and used river hydraulics simulation software by practitioners. But, HEC-RAS accounts

for debris only against piers. Unfortunately, there is no option to model debris against decks (Brunner, 2016). Commonly, entrapped driftwood ~~large woods~~ against bridge decks is ~~are~~ simulated changing the deck's geometry by lowering the girder soffit (Parola et al., 2000). Other studies consider the deposition of ~~large~~ floating woods~~s~~ on abutments instead, thus reducing the span length of the structure (Ruiz-Villanueva et al., 2013). Only in those specific cases, HEC-RAS allows to include a blocking obstacle.

A first challenge addressed here is to merge deterministic numeric tools such as HEC-RAS in a probabilistic framework, including changes in the bridge geometry to simulate driftwood clogging. This study covers this gap using the HEC-RAS Controller feature and implementing Python routines to simulate: (i) the clogging process in a single span bridge, (ii) the incremental water elevation, and (iii) the fragility curves generation through fitting the results of a Monte Carlo analysis.

3. Methodological assumptions

This Section illustrates the assumptions of the proposed method and key concepts, such as hydrodynamic coefficients and driftwood blocking probability, quantifying their role in the definition of fragilities.

3.1 Assumptions

The proposed model analyses the interaction of a bridge with the riverine environment based on the following assumptions: (i) this analysis focuses on the superstructure of the bridge, while scour effects on piers and abutments are considered out of scope; (ii) the bridge is simulated as a rigid body (Oudenbroek et al., 2018); (iii) the failure event uses Boolean metric, as the limit states domain originates from the assumption of unknown or absent bearings. This perspective often occurs in existing single span bridges, in which bearing configuration does not account for lateral restraints

or shear keys which might prevent the sliding of the structure (Sassu et al., 2017); and (iv) the hydraulic analysis is based on a 1D HEC-RAS model, even if a more refined analysis can be easily included by performing 2D modelling in HEC-RAS in cases of more complex river geometries and substantial deviations of the flow from prevalent 1D dynamics. However, the use of a 1D model for wood logs accumulation should be avoided due to the complex interaction between the driftwood and the deck. Thus, in the present work, data from actual flume tests is employed to account for reliable blocking probability estimates, as per Section 3.3. Choice of the flow representation (1D or 2D) is also related to the amount of available data in representing the river geometry (e.g. from lidar surveys instead of more traditional cross-section type of survey), while the structure of the framework remains unaltered.

3.2 Hydrodynamic Coefficients

Hydraulic actions on a submerged or partially submerged bluff body can be divided into static and dynamic components. The static part acting ~~computed forces~~ on the deck can be ~~are depleted of the static part, easy to~~ easily estimated based on water elevation. Then, the dynamic portion is decomposed into the horizontal and vertical components, called 'drag' (F_D) and 'uplift' (F_L) respectively, shown in Figure 1. A moment (M_{cg}) accounts for the distance between the force's line of action and the centre of mass of the body.

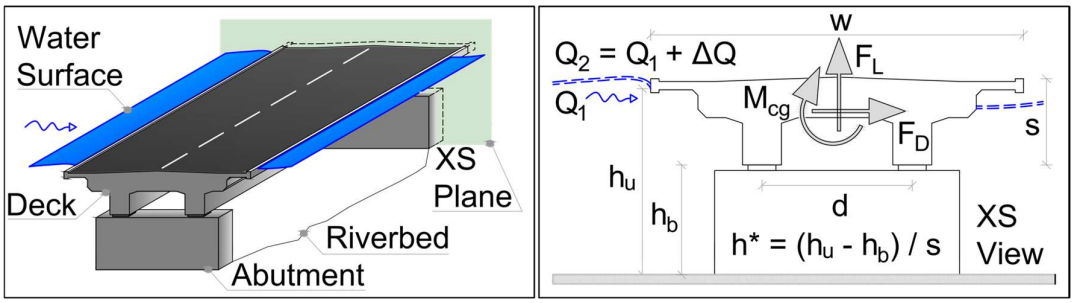

Figure 1. Bridge Deck elements (left) and forces schematics in a cross-section (XS) view (right). For representation purposes, river embankments, wing walls and approach ramps of the bridge are omitted. These elements are intended to be adjacent to the bridge abutments. Inundation Ratio indicated as h^*. Q_1, Q_2 represent water discharges, h_u and h_b symbolise the water and the deck elevation, respectively. Deck thickness is indicated as s, width as w and the bearing distance as d.

The hydrodynamic coefficients (C_i) are defined as the ratio between the acting force (F_i) and the kinetic energy density:

$$C_i = F_i / 0.5 \rho_w V_u^2 A \qquad (1)$$

Where $i = \{D, L\}$ indicates drag and uplift respectively, ρ_w is the water density, which may vary by non-negligible amounts due to flow turbidity, V_u is the approach upstream water velocity and A is the projected area of the body in the direction of F_i. The moment coefficient M_{cg} is the overturning moment to the deck's centre of gravity and w is the width of the deck:

$$C_m = M_{cg} / 0.5 \rho_w V_u^2 A w \qquad (2)$$

Studies on hydrodynamic forces led to formulations included in Standards, such as AASHTO (AASTHO, 2012), Eurocode (CEN, 2005), AS5100 (Committee BD-090, 2017) and Guidelines as FHWA Report HRT-09-028 (Kerenyi et al., 2009), CIRIA Manual (Kirby et al., 2015) among others. Differences exist between Codes on the quantification of the above coefficients. The advantage of using AASHTO or Eurocode compared to FWHA and AS5100 is linked to computational cost, having a constant drag coefficient, dynamic thrust considered as independent from water elevation, uplift and overturning components as absent. Nevertheless, easier formulations may be problematic

in several aspects, e.g. how to account for an increased thrust on foundations due to negative uplift force on partially submerged decks or, perhaps more critical, how to decide if uplift and overturning mechanisms are relevant to the bridge (Tubaldi, Macorini, & Izzuddin, 2017). Several multi-hazard frameworks included drag actions as for AASHTO (Li et al., 2020). In addition, most of the current approaches to derive flood fragility curves do not account for variable hydrodynamic coefficients. Indeed, hydrodynamic coefficients do not follow a monotonic increase with water levels and hence the critical condition could appear for discharges lower than the standard 200-years return period. This work uses the results of the Report HRT-09-028 of FHWA, because Kerenyi et al., (2009) employed CFD simulations to reproduce their experimental results extending the range of tested conditions. Drag, lift and moment coefficients are provided as functions of a parameter called 'inundation ratio', taken as the difference between the water's free surface and the bridge clearance, divided by the deck thickness (Figure 1). As indicated by (Kerenyi et al., 2009) the drag coefficient assumes values at around 2 for $h^* \approx 0$, showing a decreasing trend up to $h^* \cong 0.8$, at incipient deck's overtop. Then, the drag coefficient start to increase, up to around 2 for $h^* \geq 1.5$. While the drag coefficient is always positive, the lift one depicted negative values (for I-girders decks), acting as a stabilising force, reaching values of about –1.5 at $h^* \cong 0.9$. Then, the lift coefficient turns close to zero for $h^* > 3$. The moment coefficient is negative in the interval $0.25 < h^* \leq 1.5$, corresponding to a counter clockwise rotation of the deck, with notation of Figure 1. The opposite behaviour occurs for $h^* > 1.5$. Different curves exist in relation to the bridge width, w, as this affects the water profile beneath the lowest deck chord and the consequent applied forces.

3.3 Driftwoods Clogging Probability

The driftwood clogging at bridges may be represented as a random process that depends on several variables. Experiments conducted in the last decades shed lights on the process, including equations to estimate the backwater rise due to LW (Schalko et al., 2018, 2019). ~~Categorical probabilities are employed to account for the clogging probability.~~ Different test campaigns agree on the most influencing factors for the process, which are the congested transport of wood~~s~~ logs, low freeboard at bridges, decks with exposed structural elements characterized by sharp edges (De Cicco et al., 2020).

Many studies focused on the clogging process at bridge piers (De Cicco et al., 2018), while fewer accounted for the log entrapment at bridge decks. Among these, two studies computed the clogging probability of a single and multiple logs. Categorical probabilities are employed to account for the clogging probability. The research carried out by Schmocker and Hager (2011) parameterized the probability as a function of the bridge (B) and log lengths (L), log diameter (D_L) and flow depth (h). The driftwood orientation does not influence the clogging probability when the bridge deck is the only obstacle; this is opposed to what occurs at piers. The clogging probability for a single log is expressed by (Schmocker & Hager, 2011):

$$P_M/P_{LM} = -0.074 + 0.88\, L\,(h + 0.5D_L)/BH \tag{3}$$

In which H is the bridge clearance, P_{LM} is the maximum clogging probability tested at three relative flow depths (h/H = 0.9, 1.0 and 1.07). In the scope of this work, it is used a variable flow depth and hence, the blocking probability can be assessed only at three relative water stages *h/H = {0.9, 1.0, 1.07}*. Although interpolation it is possible, results show relative elevations well above h/H = 1.07, as per the case-study section, and therefore extrapolation is not considered.

This limitation is not present in the research of (Gschnitzer et al., 2017). The authors performed a logistic regression to compute the clogging probability of logs, based on seven predictor variables: (i) *L/B*, (ii) *h/H*, (iii) the channel gradient *i*, (iv) the smoothness of logs, (v) single or multi-span bridges, (vi) the presence of a deflecting baffle and (vii) the driftwood transport condition (either single or congested logs). ~~Further details will be provided in Section 4.~~ The clogging probability of logs can be expressed as (Gschnitzer et al., 2017):

$$P = 1/\left(1 + e^{-(\beta_1 x_1 + \beta_2 x_2 + \cdots + \beta_7 x_7)}\right) \qquad (4)$$

Where β_i are the regression coefficients and x_i the predictor variables. Comparing the two equations, the one from Gschnitzer et al., (2017) predicts a lower clogging probability for $h/H > 0.95$. This comparison is made on the reference case-study shown in the paper of Schmocker and Hager (2011). Although this result can be computed for all regimes, the limitations on *h/H* setups on the Schmocker and Hager research allow for a point comparison only. A difference of 18% in blocking probability can be observed by applying Equation (3) and (4) to the setup of Schmocker and Hager for $h/H = 1$. The parameters used for this comparison are the following: $Fr = 0.8$, $h/H = 1$, $L = 10m$, $B = 9.5m$, $D_L = 0.5m$, $H = 2.3m$, $i = 0.07$. With the mentioned values, Schmocker and Hager (2011) reported a blocking probability of the single log equal to 0.48, while using the formulation of Gschnitzer et al., (2017), it resulted 0.39, which corresponds to a 18% variation. Hence, in the present study Equation (4) is employed to characterise the clogging process mainly due to ~~given~~ the wider range of *h/H* tested. Beside this point comparison, by using Equation 4 and investigating a driftwood with branches, the clogging probability raises up to 0.85, a 54% increment. Although the effect of branches is measurable, research on wood density and therefore its buoyancy is still under

development. Ruiz-Villanueva et al., (2016) reported densities ranging from 600kg/m^3 (± 200 kg/m^3) to 800 kg/m^3 (± 170 kg/m^3), with buoyancy levels ranging from 18-30% for the denser category (green wood) to 25-44% for instream stored wood (Ruiz-Villanueva et al., 2016). These values, applied to the setup as previously discussed (0.5m), resulted in an emerging dimension between 9cm to 22cm. It was therefore deemed more safe to consider wood logs with the lowest rising height, as the wood density measurement was out of scope within the work of Gschnitzer et al., (2017). Additional details are provided in Section 5.

4. Stochastic Vulnerability Analysis

The method's workflow is summarised in Figure 2. The process starts with HEC-RAS hydraulic models similar to those used by practitioners. The hazard is characterised through an existing hydrologic model and gauge station statistics (Ercolani & Castelli, 2017). Then, the hydrodynamic coefficients are computed at each water stage, while the discharge is iteratively increased. Then, based on the knowledge of the investigated bridge, assumptions on the stochastic parameters are considered. Subsequently the drag, lift and overturning limit states are computed. Then, through Monte Carlo simulations fragility curves are obtained. The analysis of clogging scenarios requires the updating of previous tasks; specifically, the HEC-RAS bridge geometry is iteratively modified to simulate the accumulation of logs against the bridge deck. To this end, during each simulation the bottom chord of the girder is progressively lowered to simulate the entrapped driftwood, artificially increasing the deck's thickness. For each different geometry a new fragility curve can be drawn and the failure path is contained in the three-dimensional space: Failure probability - Discharge - Amount of accumulated driftwood (cross-sectional increased blockage). The automatized routines used to control HEC-RAS are based on the work of (Goodell, 2014), adapted to Python language as shown in the

work of (Dysarz, 2018). The Python scripts developed in this work are also written in Visual Basic for Application (VBA) for comparison and validation purpose. Section 4.1 illustrates the method in detail, whereas Section 4.2 describes the limit states and Section 4.3 presents the procedure to obtain the fragility curves.

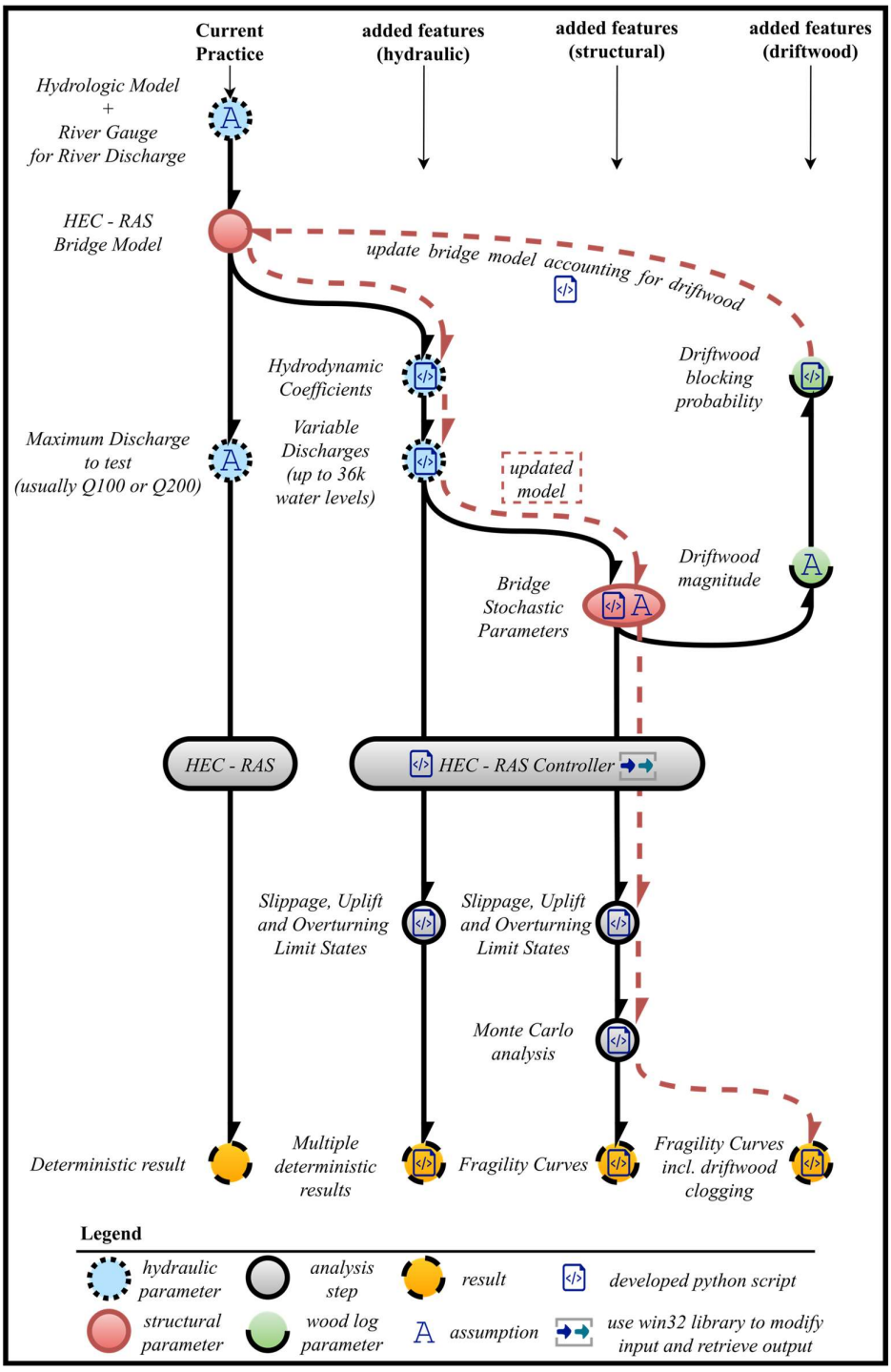

Figure 2. Workflow of the proposed method.

4.1 Methodology

The framework shown in Figure 2 is valid for single span bridges and is based on the hypotheses outlined in Section 2. The failure model considers sliding, uplift and deck overturning observed during actual floods and flume experiments (Oudenbroek et al., 2018). The stochastic variables are associated to a previous survey methodology tested on 71 bridges (Pucci et al., 2019). Indeed, the deck weight is a source of uncertainty in the case study described in Section 5, due to missing original design sheets and measurements errors. Literature data allowed for the probabilistic characterisation of the deck weight based on the span length, bridge material and typology (Petrangeli, 1996). This uncertain parameter, which strongly depends on the design practice and on the codes adopted in each Country, is taken from Petrangeli (1996) for an Italian construction site. Then, a Monte Carlo simulation is used to sample the deck weight distribution to include it in the limit state equations. Then, each value of water depth, velocity, discharge and Froude number is retrieved to compute the associated hydrodynamic coefficients and hydraulic load on the bridge. The hazard return period is independent from the progress of the framework, because the variable water depth achieved with the combined use of HEC-RAS and Python, allows to compute the hazard curve after the hydraulic simulations. The method can be seen as a lookup table approach, in which simulations are run just once. To better clarify this point, if for example one has computed discharges from 1 m^3/s to 500 m^3/s with steps of 0.1 m^3/s, this is 4990 HEC-RAS flow stages to analyse and can be done in a single run with the help of Python scripting. Then, aside from HEC-RAS computations, based on the results of a selected hydrologic model, one can find that the 200-year return period flood is associated with a 250 m^3/s value. But, when among others climate change effects are accounted for in the hydrologic model,

another discharge value should be considered for the same mean annual exceedance frequency, for example 275 m^3/s. The whole hydraulic simulation is therefore still valid, as the new discharge (275 m^3/s) is within the range $1m^3/s$ - $500m^3/s$ of previously simulated flow stages. It can be concluded that keeping the physical model separated from the probabilistic hazard characterisation allows to increase the cost-effectiveness of the method. Hence, both capacity and resistance are included in limit states equations and the probability of failure is computed as:

$$P_f = P(\, g(x) \leq 0 \mid h^* = h_i^* \,) = \left[\left(\sum_{c=1}^{N_{tot}} N_c\right)/N_{tot}\right]_i \quad (5)$$

Where $g(x)$ is a generic limit state function and h_i^* the i-th inundation ratio (Figure 1), $h_i^* = (h_{ui} - h_b) / s$, for $i = \{0, 1, \ldots, n\}$, in which n is the number of flow discharges simulated, h_{ui} the upstream water elevation, h_b the bridge clearance and s the deck thickness. $N_c = 1$ if $g_k(x) < 0$ (corresponding to bridge failure), whereas $N_c = 0$ if $g_k(x) \geq 0$. N_c and N_{tot} are the generic and the total number of simulations, for a given h_i^*. The fragility curve is then computed by using the maximum likelihood method by fitting the probabilities obtained from Equation (5) for all the tested ranges of discharge (see Section 4.3). HEC-RAS simulations are carried out in a steady-flow regime, given that the hydrodynamic effect is evaluated by using Equation (1) and (2). The current method is tailored to single-span bridges only, as the presence of a pier in combination with driftwood, can be modelled using the dedicated existing tool within HEC-RAS. What is currently missing within the software's capabilities, is the clogging process against single-span decks. Therefore, the method is repeated for different bridge geometries accounting for the ~~debris~~ driftwood effect, which is equal, as a worst-case scenario, to lowering the bottom chord of the upstream face of the deck. Hence, the driftwood clogging ~~debris accumulation~~ is a sequential damage state.

4.2 Limit States

Limit states (LS), *g(x)* consist of supply *s(x)* minus demand *d(x)* equations, i.e. *g(x) = s(x) - d(x)*, applied to the deck system of Figure 1. The streamflow force acts on the deck with an unknown direction. Hydrodynamic coefficients, as discussed in Section 3.2, can assume positive and negative values, in order to account for the thrust direction. For example, although it is common to assume that the uplift force has a positive upward direction, in the first stages of partial submersion of the deck the corresponding coefficient, C_L, is negative (Kerenyi et al., 2009). This implies a downward force, which in turn translates in greater normal force on bearings and foundations. This dynamic component interacts with the static one.

Hence, static and dynamic components of the flow may lead to the deck failure by: (i) dislodging the girder from its position with a sliding mechanism (drag), (ii) uplifting the deck due to the interaction of buoyant and dynamic uplift forces, (iii) overturning the deck due to the uneven distribution of drag and uplift with respect to the deck centre of gravity. The three LSs are treated as simultaneous, because the equations consider static and dynamic components of the flow. This is further highlighted when deriving fragility functions. Drag, uplift and overturning equations are defined according to Equation (1) and (2) reported in Section 3.2. In the following equations the drag, lift and moment components are indicated as F_{Di}, F_{Li}, M_{cgi} respectively. The subscript $i = \{1, \ldots, n_Q\}$, having n_Q as the number of flow profiles set in the HEC-RAS simulations. The slippage mechanism S_{Lij} occurring by sliding at the bearing interface is expressed by Equation (6), where $j = \{1, \ldots n_{MC}\}$; n_{MC} is the number of iterations performed by the sampling algorithm in the Monte Carlo analysis.

$$S_{Lij} = H_{ij} - F_{Di} - 0.5\,\rho_w\,g \cdot wetUP_i^2 + 0.5\,\rho_w\,g \cdot wetDN_i^2 \quad (6)$$

where g is the gravity constant, *wetUP* and *wetDN* are the wetted portion of the deck thickness and H_{ij} is the horizontal capacity against dislodging, calculated as:

$$H_{ij} = \mu\left(Fz_i - F_{Li} - B_{Ri} - B_{Ti} - \frac{M_{cgi}}{d} + \frac{B_{Ti}w}{6}d\right) \quad (7)$$

μ is the friction coefficient at the interface of the girder and the bearings, B_{Ri} and B_{Ti} are the buoyancy components according to Equation (9), d is the bearing distance as in Figure 1, w is the deck width and Fz is the deck weight evaluated as follows:

$$Fz_i = G_{sqm}L_d w_d + s_{cls}L_d w_d \rho_{cls} \quad (8)$$

G_{sqm} and s_{cls} are respectively the steelwork tonnage (kgf/m^2) and concrete volume per unit of surface (m^3/m^2) obtained from literature according to the span length and structural typology (Petrangeli, 1996). These values are included with a mean value and a standard deviation, hypothesizing a normal distribution. ρ_{cls} is the concrete density, while L_d and w_d are the longitudinal and transversal dimensions of the bridge deck.

The hydrostatic pressure can be decomposed into a rectangular and a triangular distribution due to the different water elevations upstream and downstream the bridge. B_R and B_T are given by:

$$B_R = \rho_w\, g\, w\, wetDN \quad (9)$$

$$B_T = 0.5\, \rho_w\, g\, w\, (wetUP - wetDN) \quad (10)$$

The last addendum to Equation (7) is represented by the moment generated to the deck centre of gravity by the triangular distribution of buoyancy. The uplift mechanism is generated by the balance between the deck self-weight and the algebraic sum of dynamic and static upward components of the hydraulic force. One further underlying assumption is that no vehicles are crossing the bridge at the failure time; unfortunately,

this was not always the case, as reported by previous disasters (Puppio et al., 2018), but any additional load would result in more unsafe predictions of the collapse probability due to the additional weight. Uplift LS is assessed as:

$$UP_{ij} = Fz_j - (F_{Li} + B_{Ri} + B_{Ti}) \qquad (11)$$

The overturning mechanism occurs due to the rotation of the whole deck under the water thrust. That is due to the moment given by the water thrust and the distance of its line of action from the deck centre of gravity, *CG* (Figure 1). In accordance with (Oudenbroek et al., 2018), a rotation around the rightmost bearing is assumed, having the water flowing from left to right as per Figure 1.

The vertical distance h_{cg} from the lower girder chord and the centre of gravity is calculated at each simulation, for $j = \{1, \ldots, n_{MC}\}$ by computing the static moment of the deck with respect to the lower girder chord. This was deemed necessary as the weight distribution changes at each iteration (up to n_{MC} times) in the Monte Carlo procedure. On the contrary, the horizontal distance L_{cg} from the rotation point at the rightmost bearing and the centre of gravity is supposed to remain constant, as decks are often symmetric to the x-z plane. The overturning moment is given by:

$$OV_{ij} = Fz_j L_{cg} - (F_{Li} + B_{Ri} + B_{Ti})L_{cg} + F_{Di}h_{cgi} - M_{cgi} + \frac{B_{Ti}w}{6} \qquad (12)$$

4.3 Fragility analysis

A fragility curve (FC) is, according to Equation (13), the cumulative distribution function representing the failure probability of a given structure or exceedance of a specific LS. In this paper, it is computed as the conditional probability of exceeding a certain damage state *DS* when a specific hazard magnitude im_i occurs.

$$P[\,DS \geq ds_k \mid IM = im_i\,] = \Phi\left(\frac{\ln(q_i)\mu_k}{\beta_k}\right) \quad (13)$$

q_i are the discharges included in the HEC-RAS simulations, $IM = Q$ river discharge and ds_k for $k = \{1,2,3\}$ representing the damage states associated with the three limit states defined in Section 3.2. In this work, the failure is treated as a Boolean event in Equation (5) and the associated probability is therefore categorical. The probabilities of failure are obtained by parameterizing FCs considering a lognormal distribution where μ_k and β_k are its mean and standard deviation respectively.

The LS are computed according to Equations (6), (11) and (12). Then, the outputs are included in Equation (5). The curve is therefore fitted to the observed probability of failure by using the maximum likelihood method (Baker, 2015). The final fragility curve is obtained from Equation (13).

The relationship between the collapse probability and the return period can be found by integrating the joint probability density function and considering that $1/Tr = p(Q)$, as follow:

$$P(\,DS \mid Tr\,) = \int p(\,DS \mid Q\,)p(Q)dQ \quad (14)$$

$$T_r(Q) = C_1 e^{C_2 Q} \quad (15)$$

In them, $p(DS \mid Q)$ is the probability density function of fragility, C_1 and C_2 are two constants to be determined based on extreme-value distributions on historical series of discharge data at river gauge stations (Herschy, 2019). Thus, the hazard annual exceedance frequency can be recomputed based not only on actual river flow data, but also on future trends.

The impact of driftwood~~s~~ is accounted considering its ~~their~~ entrapment probabilities $p(D)$ and new HEC-RAS geometries. The fragilities associated with the

updated bridge geometry are the conditional probabilities *P[DS / Q*]*, where *Q* = f(h, D, Q)* depends on bridge geometry, driftwood dimensions and river discharge. This function is implicitly accounted for when merging the hydraulic model with the inputs deduced from the driftwood model and the rainfall events (i.e., hydrologic model). In these occurrences, the fragilities include the driftwood occurrence as a certain event, i.e., *(p(D) = 1)*, while *p(D)* shows that the blocking probabilities are below 1 for most occurrences (see Section 3.3). Hence, to include the marginal *p(D)* within the updated fragilities, the following equation is used:

$$P[\, DS \geq ds_k \,,\, D = d_m \mid Q^* \,] = \frac{\left(p(DS,\, D{=}d_m \cap Q^*)\right)}{\left(\int p(DS,\, D = d_m \cap Q^*) dQ^*\right)} \quad (16)$$

$$P(\mathrm{DS},\, \mathrm{D} = \mathrm{d_m} \cap Q^*) = p[DS^* \mid Q^*]\, p(Q^*)\ and\ p(Q^*) = p(D|Q) = p(D) \qquad (17)$$

Equation (17) is valid because *p(D)* and *p(Q)* are independent events; i.e., the log entrapment is not a function of the flow discharge: see Section 3.3, Equation (4). Then, one can substitute the *Q** with *Q* because the new geometries are tested on the same set of discharges which are independent from the driftwood clogging probability. In addition, both structural and hydraulic models included the effect of the modified geometry at each sequential clogging event. Indeed, *p[DS* / Q*]* considers the modified geometry and *DS** refers to the clogging event d_m, while the subscript *k* is maintained for the three LS, i.e., slippage, uplift and overturning. The new family of FC is obtained with Equation (16) and can be plotted for each *k*-th mode of failure on the space Failure Probability – Discharge – Blockage Ratio, where the latter is defined as the ratio of the occupied to the free cross-section area. The failure path is therefore not unique for each bridge as it depends on the sequence of clogged logs against the bridge deck. Sequential probabilities in Equation (18) are separately evaluated for each mode of failure. The occurrence

probability of changes in wood jam upstream the bridge deck is evaluated for a given LS (i.e., fixed d_k) to follow the influence of successive entrapped logs.

$$P[\,DS = d_k,\, D = d_m \mid Q\,] = P[\,DS \geq d_k,\, D = d_m \mid Q\,] - P[\,DS \geq d_k,\, D = d_m + 1 \mid Q\,] \quad (18)$$

5. Application

The method proposed in this work is applied to a bridge located in Carrara, Tuscany, Italy.

The case-study bridge is located in via Menconi, spanning above the Carrione creek, a 46 km^2 basin, ending into the Mediterranean Sea. In 2003 a flood overtopped the via Menconi bridge and the authorities decided for its reconstruction, widening and deepening the river's cross-section by 3.8 and 1.2 m respectively. The new bridge, considered in the present study, was built in 2007, but recent flood events proved the bridge inadequate performance facing low clearances, being at risk of overtopping. Eventually, in 2021 the bridge owner decided to replace it. Back in 2007, the hydraulic study reported 425.1 m^3/s for the 200 year return period. In 2014 a new study commissioned by Regione Toscana reported a 459.6 m^3/s using the MOBIDIC Model developed by Castelli (Castelli et al., 2014). Ultimately, an updated peak discharge of 437.9 m^3/s following a recalibration of MOBIDIC was indicated.

Figure 3. Case-study bridge. Built in 2007. Demolished in 2021.

The bridge consists of a composite steel-concrete deck, with 60 cm tall I-girders connected through studs to a concrete cap of about 20 - 25 cm. The design sheets were not available and only overall external dimensions of the deck were provided from the inspection campaign in 2018 (Pucci et al., 2019). Therefore, the self-weight of the deck was unknown. This led us to hypothesize it according to the available measurements, structural typology and span length. The bridge is 10.4 m wide, spanning 19 m between the bearings. Literature data of similar bridges suggested mean value (μ) and standard deviation (β) of steelwork tonnage as $\mu = 250$ kg/m^2 and $\beta = 50$ kg/m^2 and a concrete incidence as $\mu = 0.3$ m^3/m^2, $\beta = 0.1$ m^3/m^2 (Petrangeli, 1996).

For the sake of computational cost, the steel railing was not considered as an active part of the 1D HEC-RAS model. This assumption underestimates the blockage effect during the transition of the flow above the deck. However, overtopping water forces combined with debris lead to the collapse of steel parapets before any of the investigated limit states would occur. On the contrary, reinforced concrete parapets play a major role in adding a fictitious thickness to the deck that should not be neglected (Puppio et al., 2018). The bridge of Figure 3 is part of a wider HEC-RAS model built upon request of Regione Toscana. The model was provided under license from Regione Toscana; as such, additional details can be provided by the corresponding department ("Direzione Difesa del Suolo e Protezione Civile") at local authority. The whole Carrione's reach within the floodplain is considered in the model. All the bridges spanning over the river are modelled in HEC-RAS and therefore interfering effects such as backwater rise are included in our computations.

As per hydrologic model it is used MOBIDIC, having the two mentioned calibrated datasets as inputs for the discharge computation. The hydraulic model is a 1D HEC-RAS geometry, sufficiently accurate to describe the river's behaviour. The hydrodynamic and driftwood coefficients are retrieved from FHWA (Kerenyi et al., 2009) and (Gschnitzer et al., 2017), respectively.

The limit states Equation (6), (11) and (12) are developed according to the rigid-body hypothesis used in hydrodynamic flume experiments (Kerenyi et al., 2009; Oudenbroek et al., 2018). These equations are valid if no lateral restraint systems are placed; on the contrary, a shear failure mechanism shall be accounted for when the lateral movement is forbidden (e.g., through shear keys). The actual bridge might have such restraints, as it was not possible to determine the type and properties of installed bearings. As such, only Equation (6) might not reflect a possible failure mechanism for the actual structure. Nevertheless, the validity of the framework can be demonstrated with this dataset, having the non-trivial advantage of a calibrated hydraulic and hydrologic model.

Several scenarios are tested with a newly in-house developed software tool able to interact and modify inputs to HEC-RAS geometry and flow, incorporating also the probabilistic model. The discharge interval which balanced accuracy and computational cost for the present case-study are 150 m^3/s and 600 m^3/s as initial and final flow values. The stepwise flow increment is 1 m^3/s. The HEC-RAS outputs include water surface elevations and velocities of upstream and downstream cross sections of the bridge. Then, for each HEC-RAS flow step, a Monte Carlo analysis with 20k simulations of bridge weights is performed. Limit states and fragility curve generation are computed according to Equation (6), (11), (12) and (13), respectively. As Hydrodynamic Coefficients vary with height and velocity, their values are computed for each HEC-RAS output table. Hence, a total of 9 million unique combinations of deck weight – river discharge are input

for the limit states computation. To keep the computational cost under control, a linearization of the three failure domains near the zero of each limit state function is performed and only this value written in the output file. The procedure is double-checked with two independent languages (Python-based and VBA-based) under the current ranges of tested flows, to ensure accuracy and consistency in results. The fragility curves have the mean and standard deviation values, in m^3/s and according to Equation (13), as follow: Slippage (μ = 308.941; β = 0.020), Overturning (μ = 365.646; β = 0.045), Uplift (μ = 420.074; β = 0.109). These fragility parameters are used to derive Figure 4.

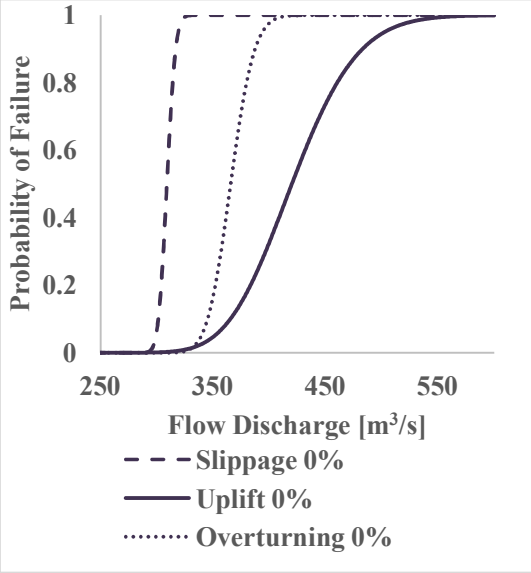

Figure 4. Fragility curves for the three limit states without the influence of clogged driftwood.

The three failure mechanisms occur simultaneously as part of the same force. Therefore, if the first limit state occurs, then the structure fails. In the case-study, the slippage is the most critical.

Then, the driftwood ~~wood log~~ blocking probability it is computed for each water surface elevation, using Equation (16). The resulting fragility curve does not follow a normal distribution, as the wood log entrapment probability follows a logit model. Accounting the most severe limit state – slippage – the same 9 million simulations are

run for different blockage ratios, namely: 10%, 20%, 30%, 40% of the bridge clearance being occupied by clogged driftwood; where the blockage ratio is the ratio between the clogged area and the one without the reduced clearance. When the blockage ratio equals 0.20, it corresponds to the unclogged scenario, where only the deck's thickness is the only obstacle to the river flow, i.e., 0.91m / (3.6m + 0.91m) = 0.2. According to Section 3.3, the first driftwood accumulation was hypothesised being 9.1cm, corresponding to a deck's thickness increment of Δs = 10%. Successive entrapped logs follows the same principle, resulting in driftwood clogging thicknesses of 9.1cm (Δs = 10%), 18.2cm (Δs = 20%), 27.3cm (Δs = 30%), 36.4cm (Δs = 40%) given by a sequence of log entrapments.

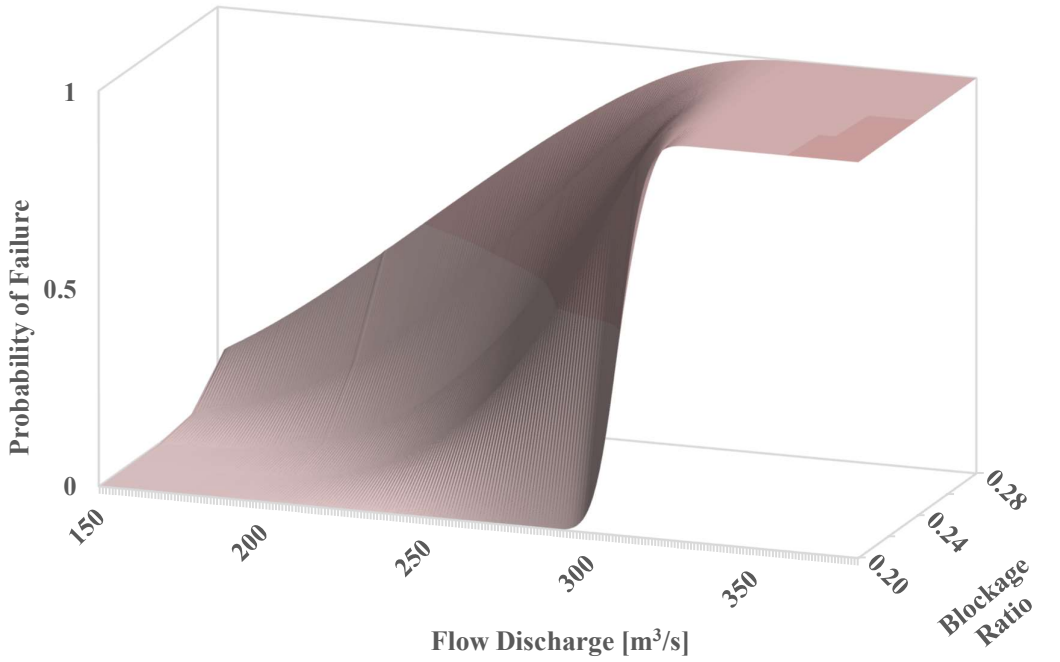

Figure 5. Interpolated surface of fragility curves for the tested scenarios ~~clogging events~~. Blockage ratio 0.20 equals the case of no driftwood, while the other values represent a progressively increased driftwood clogging situations.

Each scenario is treated with Bayesian probability, assuming at first the clogging as a certain event, while afterwards its occurrence probability is considered according to

Equation (4). The actual fragility curve lies in the space because of the log accumulation process. As expected, higher probability of failures are obtained for a given discharge in case of ~~debris~~ clogged driftwood.

Figure 6 shows that the blocking phenomenon severely affects the failure probability of the bridge and even a small reduction in clearance can result in a significant reduction of the safety of the structure. Specifically, at 298 m^3/s the failure probability without driftwood clogging is 3.3%, while it reaches 76.8% when a 9.1 cm thick log ~~wood~~ jam occurs, due to the increased hydraulic forcing experienced by the bridge deck, as the area normal to the flow increases; this value corresponds to 10% of the deck's thickness (i.e., 0.91m x 0.1 = 9.1 cm). Therefore, driftwood clogging against ~~log accumulation on~~ simply supported decks should be thoroughly investigated in both design and management of existing bridges.

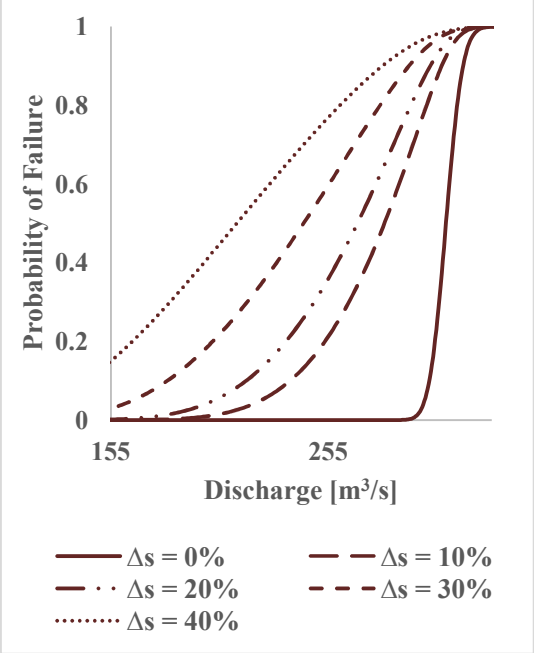

Figure 6. 2D representation of the fragility curves for different blocking scenarios as a percentage of deck's thickness increment (Δs) for slippage LS. Δs = 0% coincides with the Slippage curve of Figure 4. Each 10% addition corresponds to clogged driftwood

scenarios, resulting in Δs = 9.1cm increment of deck thickness; i.e., at Δs = 10%, the total deck thickness is: 0.91m + 0.1*0.91m = 1.00m.

The last aspect concerns the influence of the hydrologic model recalibration on the failure probability. Changes in land use as well as climate change effects on precipitation trends can lead the same discharge to have different return periods. This implies that a structure will have different safety levels on its lifespan not only due to structural aging, corrosion, among others, but also because of changes in design loads. Figure 7 shows this aspect applied to the presented case-study.

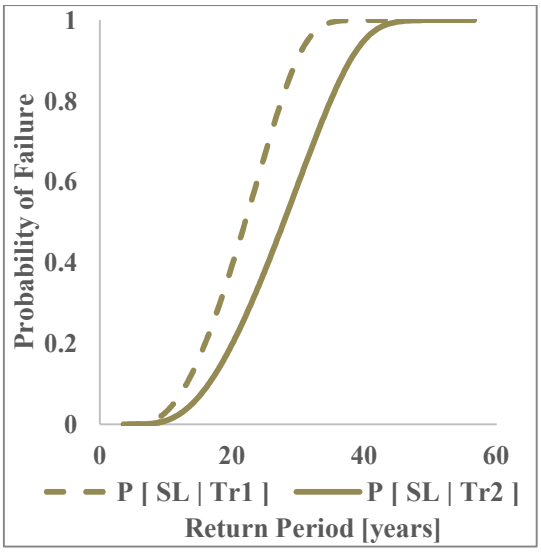

Figure 7. Influence of hydrologic model recalibration on the failure probability, for slippage limit state. Dashed line is used for the original model (Tr1), while the continuous highlights the fragility curve after model recalibration (Tr2). Therefore, P[SL | Tr_i] is the conditional probability of failure for slippage limit state (SL), given the original hydrologic model (Tr1) and the recalibrated one (Tr2).

According to Figure 7, a 30-year return period flood before the model recalibration would have led to a failure probability of 0.9, while after to 0.6. The same

return period matched with the following discharges, respectively: 306.1 m^3/s and 287.1 m^3/s. Hence, a decrease in peak discharge of 6.2% resulted in 33.3% decrease in failure probability. In this case, the recalibration led to lower discharges, but the same logic applies in the event of higher loads. As such, a hydrologic model recalibration plays a key-role in the structural safety.

6. Conclusions

Fragility curves provide the probability of reaching and exceeding certain limit states at a range of hazard magnitudes. At present, there is a lack on flood fragility research accounting for hydrodynamic actions against single-span decks, as the focus is usually on multi-span and mainly on piers. A significant gap in current literature concerns also the fragility of bridge decks considering driftwood clogging. But, following bridge failure events, flume experiment campaigns highlighted the role of driftwood blockage on single span bridges. This work combined the mentioned experimental results in a probabilistic framework, using HEC-RAS software and in-house scripts. The paper presented a method to derive fragility curves for single-span bridges under hydrodynamic actions and accounting for driftwood clogging probability. The paper investigated three limit states, namely slippage, uplift and overturning, highlighting the absence of the latter two phenomena in current European and American standards, although being considered in the Australian standard. It also mentioned the implications of flume experiments for the design and assessment of bridges, such as the counterintuitive negative hydrodynamic uplift ~~dynamic~~ component at early stage of submersion, which in turn increases the compressive load on foundations. From the hazard point of view, the paper highlights the key-role of hydrologic model when climatic shifts occur at catchment's level; specifically, land use or climate change effects can lead to significant differences in safety levels. At river level, hydraulic models play a key-role in identifying effects influencing

the structural response to the water forcing. Specifically, the case-study suffered not only overtop but also an increased positive uplift due to backwater effects generated by a nearby downstream structure. This effect could have been unaccounted for if no hydraulic model would have been employed. Lastly, the role of driftwood jams at bridge decks is investigated revealing a significant increase of failure probability during clogging processes.

Limitations of this work concerns hypotheses on the bearing typology and simplified clogging process, by simulating an increased deck's thickness. This assumption corresponds to a worst-case scenario, as it neglects the driftwood clogging porosity. Therefore, for a deeper analysis on driftwood clogging, it is suggested to use dedicated tools (Quiniou et al., 2022). Future developments of this work might include the influence of bridge typology and bearings, but also the variation of hydrodynamic loads for different deck shapes. This work concerns the use of single span bridges, while current literature offers valuable approaches considering piers (Dagá et al., 2018). The scour effect on abutments is also neglected, as this study focuses on bridge superstructure. Nevertheless, the present framework can be integrated in already existing approaches accounting for scour. As land use and climate change affect precipitation trends, the same discharge can have different return periods, which in turn can lead to dissimilar safety levels throughout the structure's lifespan. Overall, the findings demonstrate the importance of considering hydrodynamic forces and driftwood in single-span bridge deck's design and management.

Acknowledgements

The first, second and fourth authors acknowledge that, this work was partly financed by FCT / MCTES through national funds (PIDDAC) under the R&D Unit Institute for Sustainability and Innovation in Structural Engineering (ISISE), under reference UIDB /

04029/2020, and under the Associate Laboratory Advanced Production and Intelligent Systems ARISE under reference LA/P/0112/2020. This work was supported by the FCT Foundation for Science and Technology under Grant SFRH/BD/145478/2019.

The calibrated HEC-RAS 1D Model was provided for research purposes only by "Direzione Difesa del Suolo e Protezione Civile" of Regione Toscana. We would like to thank Ing. Gennaro Costabile and Ing. Francesco Piani for their kind help in providing the abovementioned model.

References

AASTHO. (2012). *Bridge design specifications*. American Association of State Highway and Transportation Officials.

Ahamed, T., Duan, J. G., & Jo, H. (2021). Flood-fragility analysis of instream bridges – consideration of flow hydraulics, geotechnical uncertainties, and variable scour depth. *Structure and Infrastructure Engineering*, *17*(11), 1494–1507. https://doi.org/10.1080/15732479.2020.1815226

Allen, E., Amaya, T., Chamorro, A., Santa María, H., Baratta, F., de Solminihac, H., & Echaveguren, T. (2021). Development and comparison of seismic fragility curves for bridges based on empirical and analytical approaches. *Structure and Infrastructure Engineering*, 1–15. https://doi.org/10.1080/15732479.2021.1993937

Argyroudis, S. A., & Mitoulis, S. A. (2021). Vulnerability of bridges to individual and multiple hazards- floods and earthquakes. *Reliability Engineering & System Safety*, *210*, 107564. https://doi.org/10.1016/j.ress.2021.107564

Argyroudis, S. A., Mitoulis, S. A., Hofer, L., Zanini, M. A., Tubaldi, E., & Frangopol, D. M. (2020). Resilience assessment framework for critical infrastructure in a multi-hazard environment: Case study on transport assets. *Science of The Total*

Environment, *714*, 136854. https://doi.org/10.1016/j.scitotenv.2020.136854

Argyroudis, S. A., Mitoulis, S. A., Winter, M. G., & Kaynia, A. M. (2019). Fragility of transport assets exposed to multiple hazards: State-of-the-art review toward infrastructural resilience. *Reliability Engineering & System Safety*, *191*, 106567. https://doi.org/10.1016/j.ress.2019.106567

Baker, J. W. (2015). Efficient Analytical Fragility Function Fitting Using Dynamic Structural Analysis. *Earthquake Spectra*, *31*(1), 579–599. https://doi.org/10.1193/021113EQS025M

Bizhanimanzar, M., Leconte, R., & Nuth, M. (2020). Catchment-Scale Integrated Surface Water-Groundwater Hydrologic Modelling Using Conceptual and Physically Based Models: A Model Comparison Study. *Water*, *12*(2), 363. https://doi.org/10.3390/w12020363

Brunner, G. W. (2016). *HEC-RAS, River Analysis System Hydraulic Reference Manual* (CPD-69; p. 547). USACE. https://www.hec.usace.army.mil/software/hec-ras/documentation/HEC-RAS%205.0%20Reference%20Manual.pdf

Castelli, F., Gardin, L., Caparrini, F., Ercolani, G., Mazzanti, B., Carlo, E. D., Turi, A., & Piani, F. (2014). *Implementazione modello distribuito per la Toscana MOBIDIC* (No. B2; p. 29). https://www.regione.toscana.it/documents/10180/12745809/B2_Finale.pdf/f5a1b35e-bba1-45ef-9843-9a3b268aabd6

CEN. (2005). *EN 1991-1-6:2005* (Eurocodes, p. 31). Euopean Committee for Standardization. https://eurocodes.jrc.ec.europa.eu/

Committee BD-090. (2017). *AS 5100.2:2017* (p. 137). Standards Australia. www.standards.org.au

Dagá, J., Chamorro, A., de Solminihac, H., & Echaveguren, T. (2018). Development of

fragility curves for road bridges exposed to volcanic lahars. *Natural Hazards and Earth System Sciences*, *18*(8), 2111–2125. https://doi.org/10.5194/nhess-18-2111-2018

D'Angelo, M., Menghini, A., Borlenghi, P., Bernardini, L., Benedetti, L., Ballio, F., Belloli, M., & Gentile, C. (2022). Hydraulic Safety Evaluation and Dynamic Investigations of Baghetto Bridge in Italy. *Infrastructures*, *7*(4), 53. https://doi.org/10.3390/infrastructures7040053

De Cicco, P. N., Paris, E., Ruiz-Villanueva, V., Solari, L., & Stoffel, M. (2018). In-channel wood-related hazards at bridges: A review. *River Research and Applications*, *34*(7), 617–628. https://doi.org/10.1002/rra.3300

De Cicco, P. N., Paris, E., Solari, L., & Ruiz-Villanueva, V. (2020). Bridge pier shape influence on wood accumulation: Outcomes from flume experiments and numerical modelling. *Journal of Flood Risk Management*, *13*(2). https://doi.org/10.1111/jfr3.12599

Dong, Y., & Frangopol, D. M. (2016). Probabilistic Time-Dependent Multihazard Life-Cycle Assessment and Resilience of Bridges Considering Climate Change. *Journal of Performance of Constructed Facilities*, *30*(5), 04016034. https://doi.org/10.1061/(ASCE)CF.1943-5509.0000883

Dráb, A., Duchan, D., Špano, M., Pavlíček, M., Zubík, P., & Štěpánková, P. (2019). Determination of the Hydrodynamic Load on an Inundated Bridge Deck by Measurements Performed on a Physical Model. *International Journal of Civil Engineering*, *17*(10), 1491–1502. https://doi.org/doi.org/10.1007/s40999-019-00411-8

Dysarz, T. (2018). Application of Python Scripting Techniques for Control and Automation of HEC-RAS Simulations. *Water*, *10*, 1382.

https://doi.org/10.3390/w10101382

Eidsvig, U., Santamaría, M., Galvão, N., Tanasic, N., Piciullo, L., Hajdin, R., Nadim, F., Sousa, H. S., & Matos, J. (2021). Risk Assessment of Terrestrial Transportation Infrastructures Exposed to Extreme Events. *Infrastructures*, *6*(11), 163. https://doi.org/10.3390/infrastructures6110163

Ercolani, G., & Castelli, F. (2017). Variational assimilation of streamflow data in distributed flood forecasting. *Water Resources Research*, *53*(1), 158–183. https://doi.org/10.1002/2016WR019208

Gehl, P., & D'Ayala, D. (2018). *System loss assessment of bridge networks accounting for multi-hazard interactions*. *14*(10), 1355–1371. https://doi.org/10.1080/15732479.2018.1434671

Goodell, C. R. (2014). *Breaking the HEC-RAS Code: A User's Guide to Automating HEC-RAS* (1st ed., Vol. 1–1). h2ls.

Gschnitzer, T., Gems, B., Mazzorana, B., & Aufleger, M. (2017). Towards a robust assessment of bridge clogging processes in flood risk management. *Geomorphology*, *279*, 128–140. https://doi.org/10.1016/j.geomorph.2016.11.002

Hamill, L. (1998). *Bridge hydraulics* (First). CRC Press.

Han, X., & Frangopol, D. M. (2022). Life-cycle connectivity-based maintenance strategy for bridge networks subjected to corrosion considering correlation of bridge resistances. *Structure and Infrastructure Engineering*, 1–24. https://doi.org/10.1080/15732479.2021.2023590

Herschy, R. W. (2019). *Streamflow Measurement* (3rd ed.). Taylor & Francis.

Kalendher, F., Setunge, S., Robert, D., & Mohaseni, H. (2018). Fragility Curves for concrete girder bridges under flood hazard. In N. Powers, D. M. Frangopol, R. Al-Mahaidi, & C. Caprani (Eds.), *Maintenance, Safety, Risk, Management and*

Life-Cycle Performance of Bridges (pp. 2393–2399). CRC Press. https://doi.org/10.1201/9781315189390-324

Kerenyi, K., Sofu, T., & Guo, J. (2009). *Hydrodynamic forces on inundated bridge decks* (FHWA-HRT-09-028; pp. 1–48). U.S. DOT.

Khandel, O., & Soliman, M. (2021). Integrated Framework for Assessment of Time-Variant Flood Fragility of Bridges Using Deep Learning Neural Networks. *Journal of Infrastructure Systems*, *27*(1), 04020045. https://doi.org/10.1061/(ASCE)IS.1943-555X.0000587

Kim, H., Sim, S.-H., Lee, J., Lee, Y.-J., & Kim, J.-M. (2017). Flood fragility analysis for bridges with multiple failure modes. *Advances in Mechanical Engineering*, *9*(3), 168781401769641. https://doi.org/10.1177/1687814017696415

Kirby, A., Roca, M., Kitchen, A., Escarameia, M., & J.Chesterton. (2015). *Manual on scour at bridges and other hydraulic structures*. CIRIA.

Lam, J. C., Adey, B. T., Heitzler, M., Hackl, J., Gehl, P., van Erp, N., D'Ayala, D., van Gelder, P., & Hurni, L. (2018). Stress tests for a road network using fragility functions and functional capacity loss functions. *Reliability Engineering & System Safety*, *173*, 78–93. https://doi.org/10.1016/j.ress.2018.01.015

Lamb, R., Garside, P., Pant, R., & Hall, J. W. (2019). A Probabilistic Model of the Economic Risk to Britain's Railway Network from Bridge Scour During Floods. *Risk Analysis*, *39*(11), 2457–2478. https://doi.org/10.1111/risa.13370

Li, Y., Dong, Y., Frangopol, D. M., & Gautam, D. (2020). Long-term resilience and loss assessment of highway bridges under multiple natural hazards. *Structure and Infrastructure Engineering*, *16*(4), 626–641. https://doi.org/10.1080/15732479.2019.1699936

Mazzorana, B., Ruiz-Villanueva, V., Marchi, L., Cavalli, M., Gems, B., Gschnitzer, T.,

Mao, L., Iroumé, A., & Valdebenito, G. (2018). Assessing and mitigating large wood-related hazards in mountain streams: Recent approaches. *Journal of Flood Risk Management*, *11*(2), 207–222. https://doi.org/10.1111/jfr3.12316

Mondoro, A., & Frangopol, D. M. (2018). Risk-based cost-benefit analysis for the retrofit of bridges exposed to extreme hydrologic events considering multiple failure modes. *Engineering Structures*, *159*, 310–319. https://doi.org/10.1016/j.engstruct.2017.12.029

Oudenbroek, K., Naderi, N., Bricker, J. D., Yang, Y., van der Veen, C., Uijttewaal, W., Moriguchi, S., & Jonkman, S. N. (2018). Hydrodynamic and debris-damming failure of bridge decks and piers in steady flow. *Geosciences (Switzerland)*, *8*(11). Scopus. https://doi.org/10.3390/geosciences8110409

Panici, D., & de Almeida, G. A. M. (2018). Formation, Growth, and Failure of Debris Jams at Bridge Piers. *Water Resources Research*, *54*(9), 6226–6241. https://doi.org/10.1029/2017WR022177

Panici, D., & Kripakaran, P. (2023). Assessing and mitigating risks to bridges from large wood using satellite imagery. *Proceedings of the Institution of Civil Engineers - Bridge Engineering*, *176*(2), 118–128. https://doi.org/10.1680/jbren.21.00059

Parola, A. C., Apelt, C. J., & Jempson, M. (2000). *Debris Forces on Highway Bridges* (NCHRP No. 445; p. 90). Transportation Research Board. https://onlinepubs.trb.org/onlinepubs/nchrp/nchrp_rpt_445.pdf

Petrangeli, M. P. (1996). *Progettazione e Costruzione di Ponti* (IV). CEA.

Porter, K., Kennedy, R., & Bachman, R. (2007). Creating Fragility Functions for Performance-Based Earthquake Engineering. *Earthquake Spectra*, *23*(2), 471–489. https://doi.org/10.1193/1.2720892

Proske, D. (2018). *Bridge collapse frequencies versus failure probabilities* (Vol. 8). Springer.

Pucci, A., Sousa, H. S., Lucio Puppio, M., Giresini, L., Matos, J. C., & Sassu, M. (2019). Method for sustainable large-scale bridges survey. *Towards a Resilient Built Environment Risk and Asset Management - Report*, 1034–1041.

Puppio, M. L., Novelli, S., & Sassu, M. (2018). Failure evidences of reduced span bridges in case of extreme rainfalls The case of Livorno. *Frattura Ed Integrità Strutturale*, *12*(46), Article 46. https://doi.org/10.3221/IGF-ESIS.46.18

Quiniou, M., Piton, G., Villanueva, V. R., Perrin, C., Savatier, J., & Bladé, E. (2022). Large Wood Transport-Related Flood Risks Analysis of Lourdes City Using Iber-Wood Model. In P. Gourbesville & G. Caignaert (Eds.), *Advances in Hydroinformatics* (pp. 481–498). Springer Nature Singapore.

Ruiz-Villanueva, V., Bodoque, J. M., Díez-Herrero, A., Eguibar, M. A., & Pardo-Igúzquiza, E. (2013). Reconstruction of a flash flood with large wood transport and its influence on hazard patterns in an ungauged mountain basin: Woody debris in flood hazard analysis. *Hydrological Processes*, *27*(24), 3424–3437. https://doi.org/10.1002/hyp.9433

Ruiz-Villanueva, V., Piégay, H., Gaertner, V., Perret, F., & Stoffel, M. (2016). Wood density and moisture sorption and its influence on large wood mobility in rivers. *CATENA*, *140*, 182–194. https://doi.org/10.1016/j.catena.2016.02.001

Ruiz-Villanueva, V., Wyżga, B., Mikuś, P., Hajdukiewicz, M., & Stoffel, M. (2017). Large wood clogging during floods in a gravel-bed river: The Długopole bridge in the Czarny Dunajec River, Poland: Large wood clogging during floods. *Earth Surface Processes and Landforms*, *42*(3), 516–530. https://doi.org/10.1002/esp.4091

Sassu, M., Giresini, L., & Puppio, M. L. (2017). Failure scenarios of small bridges in case of extreme rainstorms. *Sustainable and Resilient Infrastructure*, *2*(3), 108–116. Scopus. https://doi.org/10.1080/23789689.2017.1301696

Schalko, I. (2018). *Modeling Hazards Related to Large Wood in Rivers* [PhD Thesis, ETH Zürich]. https://doi.org/10.3929/ethz-b-000293084

Schalko, I., Lageder, C., Schmocker, L., Weitbrecht, V., & Boes, R. M. (2019). Laboratory Flume Experiments on the Formation of Spanwise Large Wood Accumulations: I. Effect on Backwater Rise. *Water Resources Research*, *55*(6), 4854–4870. https://doi.org/10.1029/2018WR024649

Schalko, I., Schmocker, L., Weitbrecht, V., & Boes, R. M. (2017). Schwemmholz: Gefahrenbeurteilung und Massnahmenplanung am Fallbeispiel Renggbach, Kanton Luzern. *Wasser Energie Luft*, *109*(4), 271–278.

Schalko, I., Schmocker, L., Weitbrecht, V., & Boes, R. M. (2018). Backwater Rise due to Large Wood Accumulations. *Journal of Hydraulic Engineering*, *144*(9), 04018056. https://doi.org/10.1061/(ASCE)HY.1943-7900.0001501

Schalko, I., Schmocker, L., Weitbrecht, V., & Boes, R. M. (2020). Risk reduction measures of large wood accumulations at bridges. *Environmental Fluid Mechanics*, *20*(3), 485–502. https://doi.org/10.1007/s10652-019-09719-4

Schalko, I., & Weitbrecht, V. (2022). Impact of Large Wood on River Ecosystems. *Water*, *14*(5). https://doi.org/10.3390/w14050784

Schmocker, L., & Hager, W. H. (2011). Probability of Drift Blockage at Bridge Decks. *Journal of Hydraulic Engineering*, *137*(4), 470–479. https://doi.org/10.1061/(ASCE)HY.1943-7900.0000319

Schmocker, L., & Weitbrecht, V. (2013). Driftwood: Risk Analysis and Engineering Measures. *Journal of Hydraulic Engineering*, *139*(7), 683–695.

https://doi.org/10.1061/(ASCE)HY.1943-7900.0000728

Spyrou, C., Varlas, G., Pappa, A., Mentzafou, A., Katsafados, P., Papadopoulos, A., Anagnostou, M. N., & Kalogiros, J. (2020). Implementation of a Nowcasting Hydrometeorological System for Studying Flash Flood Events: The Case of Mandra, Greece. *Remote Sensing*, *12*(17), 2784. https://doi.org/10.3390/rs12172784

Steeb, N., Rickenmann, D., Badoux, A., Rickli, C., & Waldner, P. (2017). Large wood recruitment processes and transported volumes in Swiss mountain streams during the extreme flood of August 2005. *Geomorphology*, *279*, 112–127. https://doi.org/10.1016/j.geomorph.2016.10.011

Tanasić, N., & Hajdin, R. (2018). Management of bridges with shallow foundations exposed to local scour. *Structure and Infrastructure Engineering*, *14*(4), 468–476. https://doi.org/10.1080/15732479.2017.1406960

Tubaldi, E., Macorini, L., & Izzuddin, B. (2017). Flood Risk Assessment of Masonry Arch Bridges. *Proceedings of the 2nd International Conference on Uncertainty Quantification in Computational Sciences and Engineering (UNCECOMP 2017)*, 140–153. https://doi.org/10.7712/120217.5358.16942

Tubaldi, E., Macorini, L., Izzuddin, B. A., Manes, C., & Laio, F. (2017). A framework for probabilistic assessment of clear-water scour around bridge piers. *Structural Safety*, *69*, 11–22. https://doi.org/10.1016/j.strusafe.2017.07.001

Van Campenhout, J., Houbrechts, G., Peeters, A., & Petit, F. (2020). Return Period of Characteristic Discharges from the Comparison between Partial Duration and Annual Series, Application to the Walloon Rivers (Belgium). *Water*, *12*(3), 792. https://doi.org/10.3390/w12030792

Wyss, A., Schalko, I., & Weitbrecht, V. (2021). Field Study on Wood Accumulation at

a Bridge Pier. *Water*, *13*(18). https://doi.org/10.3390/w13182475

Yilmaz, T., Banerjee, S., & Johnson, P. A. (2016). Performance of Two Real-Life California Bridges under Regional Natural Hazards. *Journal of Bridge Engineering*, *21*(3), 04015063. https://doi.org/10.1061/(ASCE)BE.1943-5592.0000827

Yilmaz, T., Banerjee, S., & Johnson, P. A. (2018). Uncertainty in risk of highway bridges assessed for integrated seismic and flood hazards. *Structure and Infrastructure Engineering*, *14*(9), 1182–1196. https://doi.org/10.1080/15732479.2017.1402065